Interaction of katabatic winds and near-surface temperatures in the Antarctic

Timo Vihma,[1] Eveliina Tuovinen,[2] and Hannu Savijärvi[2]

Received 17 August 2010; revised 29 August 2011; accepted 30 August 2011; published 15 November 2011.

[1] A two-dimensional mesoscale model was applied to simulate wintertime katabatic winds in the Antarctic coastal region. Simulations were made for a constant slope angle with the slope height varying and for fixed slope heights with the slope angle varying. Thermal wind opposed the katabatic flow near the foot of the slope, but enhanced it over the high plateau. The steeper and higher the slope, the stronger the effect on the plateau. The 2 m potential temperature decreased down the slope toward sea ice, because (1) the katabatic wind resulted in the accumulation of cold near-surface air over the sea ice and the lower parts of the slope, (2) over the flat sea ice zone, the stratification was stronger, and (3) the shallow slope was within the strong surface inversion from over the sea ice. With a slope aspect ratio of 5 m km^{-1} and a slope height below 1000 m, 2 m temperature (T_{2m}) decreased down the slope, but for slope heights of 1500 m and more T_{2m} increased down the slope. Adiabatic warming and, because of the stronger wind, enhanced turbulent mixing of the warmer air from aloft contributed to the warming. For slope angles ranging from 1 to 20 m km^{-1}, with a small slope height of 500 m, T_{2m} decreased down the slope but not monotonically, whereas with a slope height of 2000 m, yielding stronger winds and larger adiabatic warming, T_{2m} increased monotonically down the slope. The model results were supported by observations from several Antarctic sites with different topographic conditions.

Citation: Vihma, T., E. Tuovinen, and H. Savijärvi (2011), Interaction of katabatic winds and near-surface temperatures in the Antarctic, *J. Geophys. Res.*, *116*, D21119, doi:10.1029/2010JD014917.

1. Introduction

[2] A katabatic wind is a downslope flow driven by gravity and pressure gradient forces on a cold sloping surface, which is typically cooled by a negative radiation balance. On the large sloping glaciers in the Antarctic and Greenland, the Coriolis force becomes important and downslope flows are not pure katabatic winds [e.g., *Kottmeier*, 1986]. Here we define the katabatic wind as a downslope wind initially generated by surface cooling.

[3] Katabatic winds typically occur in the lowermost tens or a few hundreds of meters of the atmosphere; the height of the maximum wind speed is sometimes just a few meters [*Barry*, 2008] but sometimes it is 100–200 m [*Argentini et al.*, 1996]. Katabatic winds may occur in a large range of spatial and temporal scales. Local katabatic winds are developed at nighttime in mid- and low latitudes on the slopes on mountains and even small hills [*Monti et al.*, 2002]. In the case of large mountain glaciers, katabatic winds may occur also in summer and prevail through the day [*Reuder et al.*, 2011]. In the Antarctic and Greenland, katabatic winds are remarkably unidirectional and persistent [*King and Turner*, 1997]. The strongest and most persistent katabatic winds take place in the coastal sections of Adelie Land in east Antarctica: An annual mean wind speed of approximately 20 m s^{-1} was observed during Mawson's 1911–1914 Australasian Antarctic Expedition [*Parish and Wendler*, 1991].

[4] Since *Defant* [1933] and *Prandtl* [1942, 1952], hundreds of papers have addressed the dynamics of katabatic winds. The effects of katabatic winds on the air temperature have received comparatively much less focus, although many studies include some aspects of thermodynamics. *Hogan* [1997] reported that the lowest annual mean potential temperatures (θ) in the Antarctica (less than 248 K) occur on the Ross and Ronne Ice Shelves and in a small circle near the South Pole. He concluded that the reasons for the coldness of the ice shelves is the accumulation of cold near-surface air by katabatic winds. Also, the regional climate model results of *van den Broeke and van Lipzig* [2003] showed that in the case of weak synoptic-scale flow, katabatic winds resulted in piling up of air with low θ over sea ice and ice shelves. In the modeling studies of *van As and van den Broeke* [2007], a positive feedback was observed in the Antarctic summer between a low θ and the katabatic wind speed.

[5] Depending on the point of view (spatial variations or Eulerian or Lagrangian changes in time) and the observation site with respect to the slope, katabatic winds may be related

[1]Meteorological Research, Finnish Meteorological Institute, Helsinki, Finland.
[2]Department of Physics, University of Helsinki, Helsinki, Finland.

0148-0227/11/2010JD014917

to warming or cooling of the air. Considering the true air temperature (T), the sign of the change may, however, vary from case to case even if we restrict to a certain kind of observations (Eulerian, Lagrangian, or spatial). *Périard and Pettré* [1993] observed that during autumn and spring the effect of cold-air advection by katabatic winds lowered the air temperature at Dumont d'Urville, Ade1ie Land, Antarctica. In the Rocky Mountains, addressing the interaction of katabatic flow and mountain waves, *Poulos et al.* [2007] concluded that cold-air advection played an important role. Warming during katabatic winds is usually due to adiabatic warming and increased mixing in the stable boundary layer so that warmer inversion-layer air is brought down to the surface. *Streten* [1990] reported about an increase of 2 m air temperature (T_{2m}) after the onset of katabatic winds in winter at the Mawson station, Antarctica. *Parish and Bromwich* [1989] analyzed infrared imagery from the Reeves Glacier and Nansen Ice Sheet and *Bromwich et al.* [1992] analyzed it from the Ross Ice Shelf: Both studies led to the conclusion that extensive warm signatures were related to mixing due to katabatic winds. According to *Zwally and Fiegles* [1994] some snowmelt patterns during the Antarctic summer appeared to be related to katabatic wind effects. *Ohata et al.* [1982] observed that the effect of mixing due to katabatic winds suppressed the occurrence of a very stable boundary layer, thus increasing near-surface air temperatures.

[6] Our objectives are to better understand (1) the reasons for the contrasting heating and cooling events observed during katabatic winds, and (2) the feedback from the air temperature distribution to the dynamics of the katabatic flow. We simulate katabatic winds for different combinations of slope height and steepness. A two-dimensional (2-D) model, practical for a large number of idealized sensitivity tests, is applied. The model is first validated for two regions in east Antarctica (section 2). Then we study the effect of katabatic winds on the air temperature for varying slope heights (section 3), and after that we vary the slope aspect ratio for two fixed slope heights (section 4). The wind-temperature relationships are analyzed and interpreted with the help of heat and momentum budgets calculated on the basis of the model results. Section 4 also addresses hydraulic jumps. Comparisons against analytical solutions, modeling studies, and observations are presented in section 5, and conclusions are drawn in section 6.

2. The 2-D Model and Its Validation

2.1. The 2-D Model

[7] We use the University of Helsinki (UH) 2-D sigma coordinate model based on *Alpert et al.* [1982] but with improved dynamics and physics. The large-scale pressure gradient is presented via constant geostrophic wind (V_g, with components u_g southward and v_g eastward). The model physics consists here of a Monin-Obukhov lowest layer and a first-order turbulence closure, a four-band shortwave and six-band longwave radiation scheme, and a force-restore snow scheme. Moisture is predicted but the present experiments assume an initially dryish Antarctic environment without clouds actually forming. In the turbulence scheme, the vertical diffusion coefficient K depends on the local wind shear and on the local Richardson number Ri:

$$K = l^2(\mathrm{d}U/\mathrm{d}z)f(Ri), \tag{1}$$

where the mixing length is given by $l = \kappa z/(1 + \kappa z/\lambda)$, λ is its asymptotic maximum value (we use $\lambda = 30$ m) and κ is the von Kármán constant (0.4). In conditions of stable stratification, the following stability function is used for momentum, heat, and moisture [*Zilitinkevich et al.*, 2002]:

$$f(Ri) = \max\left[0.003, \frac{1}{(1 + 6Ri + 36Ri^2)^2}\right], \tag{2}$$

where the constant 0.003 represents the background turbulence in very stable conditions, preventing K from decreasing to zero. The model has produced realistic downslope, coastal, Antarctic, and Arctic winds and temperatures [e.g., *Vihma and Brümmer*, 2002; *Vihma et al.*, 2003, 2005; *Savijärvi et al.*, 2005; *Savijärvi*, 2009, 2011; *Gahmberg et al.*, 2010; these references provide details about the model and its parameterizations]. Here a 5 km grid length on 50 sigma levels is adopted, the two lowest levels being at 1.7 m (hereinafter 2 m) and 4 m and the highest at about 6 km above the sea surface. The x axis is set southward across the Antarctic coastline at about 70°S, with flat, snow-covered sea ice in the north. The thermodynamic snow properties over the sea ice and over the glacier are based on typical observed values of relatively fresh Antarctic snow, and the roughness length for momentum is 0.5 mm.

2.2. Validation Against Observations

[8] To ensure that the 2-D-model is capable of simulating realistic Antarctic wintertime conditions, the model was tested against near-surface wind and temperature observations from the research stations Dumont d'Urville in Adelie Land (66.67°S, 140.02°E) and Mawson in MacRobertson Land (67.60°S, 62.88°E). The data applied in the validation were wintertime (1 June to 31 August) synoptic observations from the years 1998–2002. The large-scale topography is rather similar near the two stations, with a steep coastal slope to 1800 m at an aspect ratio of about 15 m km^{-1} in the case of Dumont d'Urville and a slope height of 1200 m at an aspect ratio of 22 m km^{-1} in the case of Mawson. Dumont d'Urville is located in a small island less than 2 km from the coast, whereas Mawson is situated on the coast at the foot of the continental ice sheet.

[9] Both Dumont d'Urville and Mawson are in the region of strong katabatic winds. In midwinter, the observed 10-m mean wind speed is 10–12 m s^{-1} at Dumont d'Urville and the katabatic winds are commonly from the direction of 120°–140°, i.e., 40°–60° left of the local fall line (downslope to 180°) [*Turner and Pendleburry*, 2004]. Taking into consideration the anticlockwise turning of katabatic wind due to the Coriolis effect, the x axis of the 2-D model was set to point south. At Mawson the katabatic winds are mainly from the southeast [*Turner and Pendleburry*, 2004]. As in the case of Dumont d'Urville, the 2-D model fall line for the Mawson experiments was set in the north–south direction. The typical winter temperatures are near −15°C to

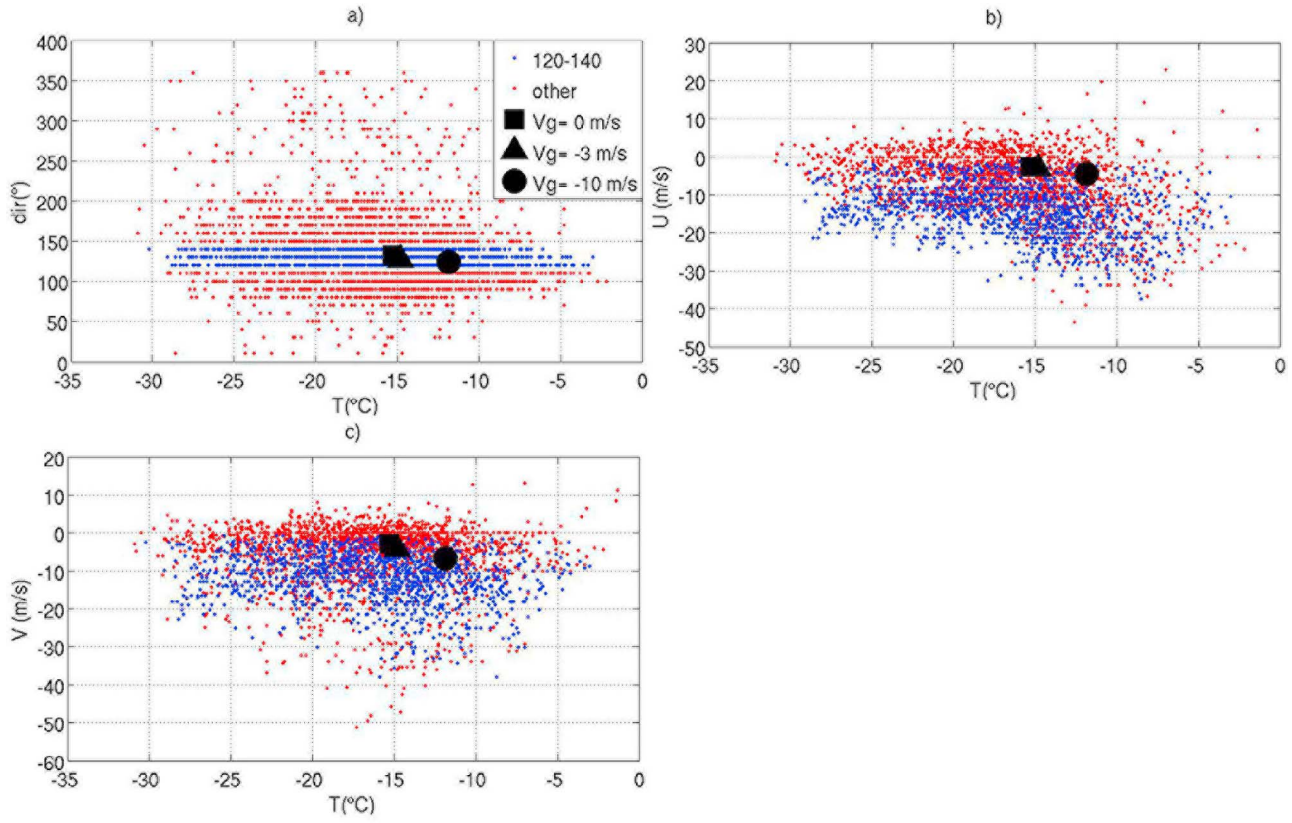

Figure 1. The observed and modeled relationships between the 2 m air temperature and (a) wind direction, (b) north–south wind component (u), and (c) west–east wind component (v) at Dumont d'Urville. The observations are from June to August 1998–2002. Blue dots represent wind observations when the flow is assumed to be katabatic. Red dots stand for wind observations in other cases. Square, triangle, and circle represent simulations where $v_g = 0$, $v_g = -3$, and $v_g = -10$ m s^{-1}, respectively.

−25°C at Mawson and −16°C to −17°C at Dumont d'Urville [*Turner and Pendleburry*, 2004].

[10] The 2-D model was tested against three different kinds of horizontally and vertically homogeneous initial wind regimes. In the first experiment the model produced the katabatic flow starting from rest (no geostrophic wind). In the second experiment, a weak easterly geostrophic wind ($v_g = -3$ m s^{-1}) prevailed, to simulate a situation of a weak pressure gradient when the downslope flow is to a great extent katabatic. The third experiment represented a low-pressure situation with a typical coastal easterly geostrophic wind ($v_g = -10$ m s^{-1}). The low-pressure center was situated over the sea north from the shore, and the geostrophic wind blew along the shore line. All the experiments represented clear-sky winter conditions without solar radiation. The simulation time was 48 h, which was enough for the wind field to reach a quasi steady state (see section 5 for information on the remaining oscillations). The results at the end of each model run were analyzed. The ERA-Interim Reanalysis [*Dee et al.*, 2011] was applied to define the initial temperature fields on the plateaus above Dumont d'Urville and Mawson. The mean midwinter temperature profile over the surface-based inversion layer (typically reaching the height of 1.1 km) was linearly extrapolated down to the surface. The extrapolated surface temperature, which was typically 20°C–30°C higher than climatological values, was applied at the lowest level of the 2-D model on the plateau, and the rest of the initial temperature field was set to be horizontally homogeneous and vertically adiabatic. Hence, the 2-D model itself had to generate the wintertime temperature inversion and katabatic winds. Via this approach, the model output was as little as possible affected by the given initial conditions, but was instead determined by the simulated thermodynamics and steady state winds of the local boundary layer.

[11] The validation results are shown in Figure 1 for Dumont d'Urville and in Figure 2 for Mawson. In the katabatic situations at Dumont d'Urville the observed mean wintertime T_{2m} was −17°C and the simulated temperatures were from −12°C ($v_g = -10$ m s^{-1}) to −15°C ($v_g = -3$–0 m s^{-1}). At Mawson the observed mean wintertime T_{2m} in the case of katabatic flow was −16°C, and the simulated temperatures were between −19°C and −21°C. Also, the modeled u and v wind components fitted well to the group of the katabatic observations. The observed mean u and v wind components at Mawson were both in the case of the katabatic flow approximately −4 m s^{-1}. The corresponding simulated u winds ranged from −4 to −2 m s^{-1} and v winds ranged from −6 to −2 m s^{-1}. Also at Dumont d'Urville the simulated u and v wind components fitted into the group of the observed wind components during katabatic situations, although they were among the weakest observed winds.

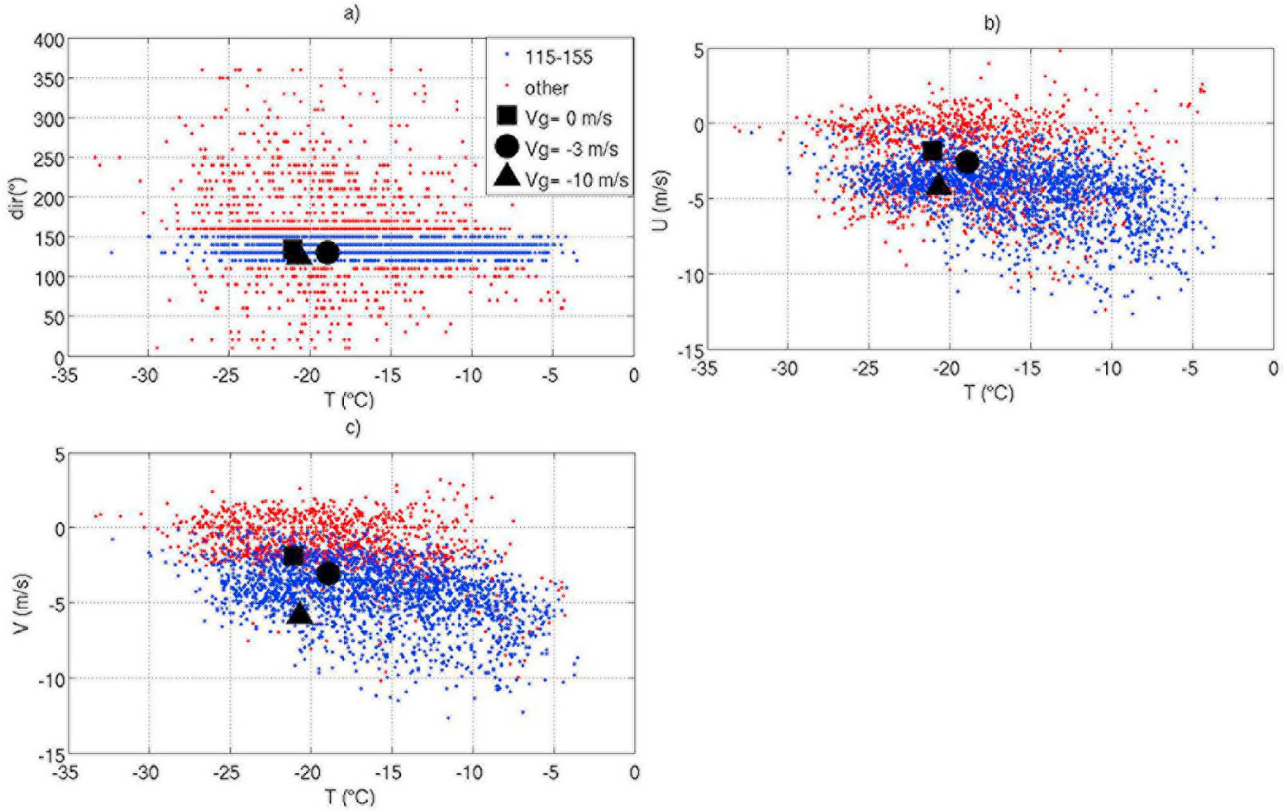

Figure 2. As in Figure 1 but for Mawson.

[12] As a conclusion, the 2-D model is able to produce realistic Antarctic wintertime conditions when the slope topography is simple enough, as in the regions of Dumont d'Urville and Mawson. Comparisons against published theoretical analyses, model experiments, and various other observations are presented in section 5.

3. The Effect of Slope Height

[13] The UH 2-D model is now applied in idealized experiments for a single Antarctic coastal slope, first focusing to the effects of the slope height. Except for the topography, the experiments are basically similar to the simulations for Dumont d'Urville and Mawson. The topography consists of 200 km of sea ice, a coastline at 67°S, a slope of variable height, and 200 km of plateau farther to the south. The slope aspect ratio (steepness) is fixed at 5 m km^{-1} (slope angle of 0.3°). This value represents a compromise between the observed steep aspect ratios near the coast (~10 m km^{-1}) and farther away from the coast ~1 m km^{-1}) [*King and Turner*, 1997]. The heights of the slope H are set to 250, 500, 1000, 1500, 2000, and 3000 m (experiments H1–H6, respectively, in Table 1). The simulations are initialized with a horizontally homogeneous atmosphere at rest. The initial temperature field is that applied in the model validation for Dumont d'Urville. There is no V_g, the relative humidity (RH) is initially 60%, and clear-sky midwinter conditions prevail. As the x axis increases to the south, the downslope wind is associated with a negative u component in the following. The resulting steady state katabatic winds and temperatures along the slope are studied.

[14] From Figure 3a we see that θ_{2m} systematically decreases toward the coast along the fall line (model x axis). Three mechanisms contribute to this: (1) The katabatic wind has resulted in the accumulation of radiatively cooled near-surface air over the sea ice and over the lower parts of the slope; (2) over the flat sea ice zone, the stratification is stronger, resulting in lower near-surface temperatures

Table 1. Topography in Various Model Experiments

Experiment	Slope Height (m)	Aspect Ratio (m km^{-1})
H0	0	0
H1	250	5
H2	500	5
H3	1000	5
H4	1500	5
H5	2000	5
H6	3000	5
S1.1	500	1
S1.2	500	3.6
S1.3	500	5
S1.4	500	10
S1.5	500	15
S1.6	500	20
S2.1	2000	1
S2.2	2000	3.6
S2.3	2000	5
S2.4	2000	10
S2.5	2000	15
S2.6	2000	20

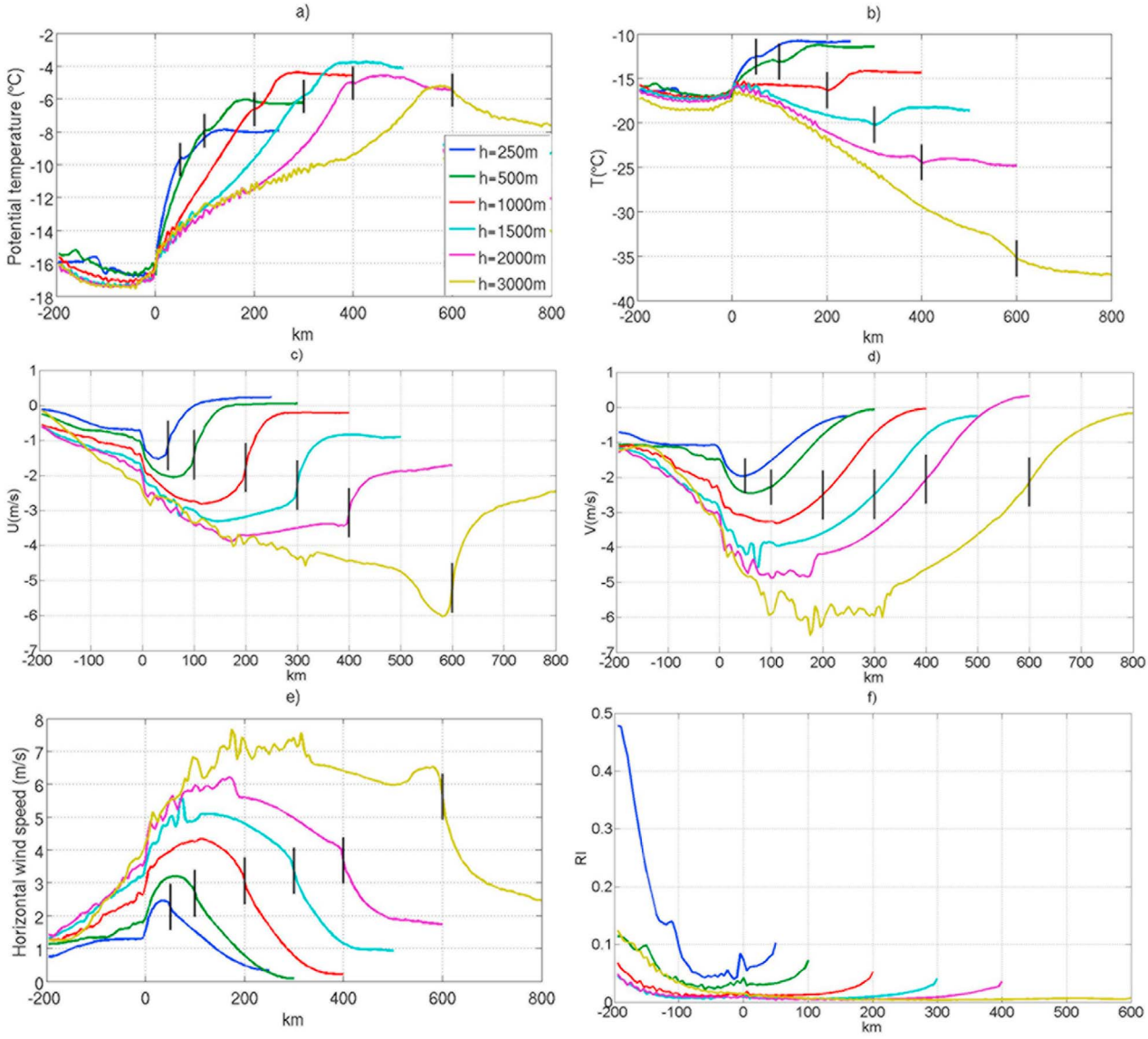

Figure 3. Results of the simulations in which the slope height varies: (a) θ_{2m}, (b) T_{2m}, (c) u_{2m}, (d) v_{2m}, (e) the 2 m wind speed, and (f) Ri_{2m}. The negative values on the x axis denote the sea ice region. The slope is situated on the left-hand side of the black vertical bar on the positive x axis; on the right-hand side is the high plateau. In Figure 3f, Ri_{2m} is plotted only on the slope and the sea ice region, not on the high plateau. Negative u in Figure 3c indicates the downslope wind component.

(Figure 4); and (3) the shallow slopes are within the strong surface inversion from over the sea ice (no katabatic wind is needed for that). θ_{2m} decreases with all slope heights, but the decrease is less rapid for high slopes with a strong 2 m wind (Figure 3e) and more turbulent mixing (Figure 3f). As the total slope height and wind speed increase, Ri_{2m} decreases and the near-surface turbulence increases at a fixed distance south of the coast (Figure 3f; Ri_{2m} was calculated from the model results at the surface and the second-lowest model level at 4 m). Over the slope and sea ice Ri_{2m} stays below 0.2, except over the sea ice in the case of the lowest slope. The most stable air is situated over the high plateau (Ri often exceeding 0.2; not shown in Figure 3f), the upper part of the slope, and the sea ice. Figure 5a shows that Ri_{2m} averaged over the length of the slope decreases as the slope height increases.

[15] To interpret the results more quantitatively, we analyze the vertical profiles of wind and potential temperature, as well as the terms of the momentum and heat budget equations. The equations are as follows (see *Mahrt* [1982] for the momentum budget):

$$\frac{\partial u}{\partial t} = -u\frac{\partial u}{\partial x} - w\frac{\partial u}{\partial z} + fv - g\frac{\Delta\theta}{\theta_0}\sin\alpha + \cos\alpha\frac{g}{\theta_0}\frac{\partial(\overline{\Delta\theta}h)}{\partial x} - \frac{1}{\rho}\frac{\partial\tau_x}{\partial z}, \quad (3)$$

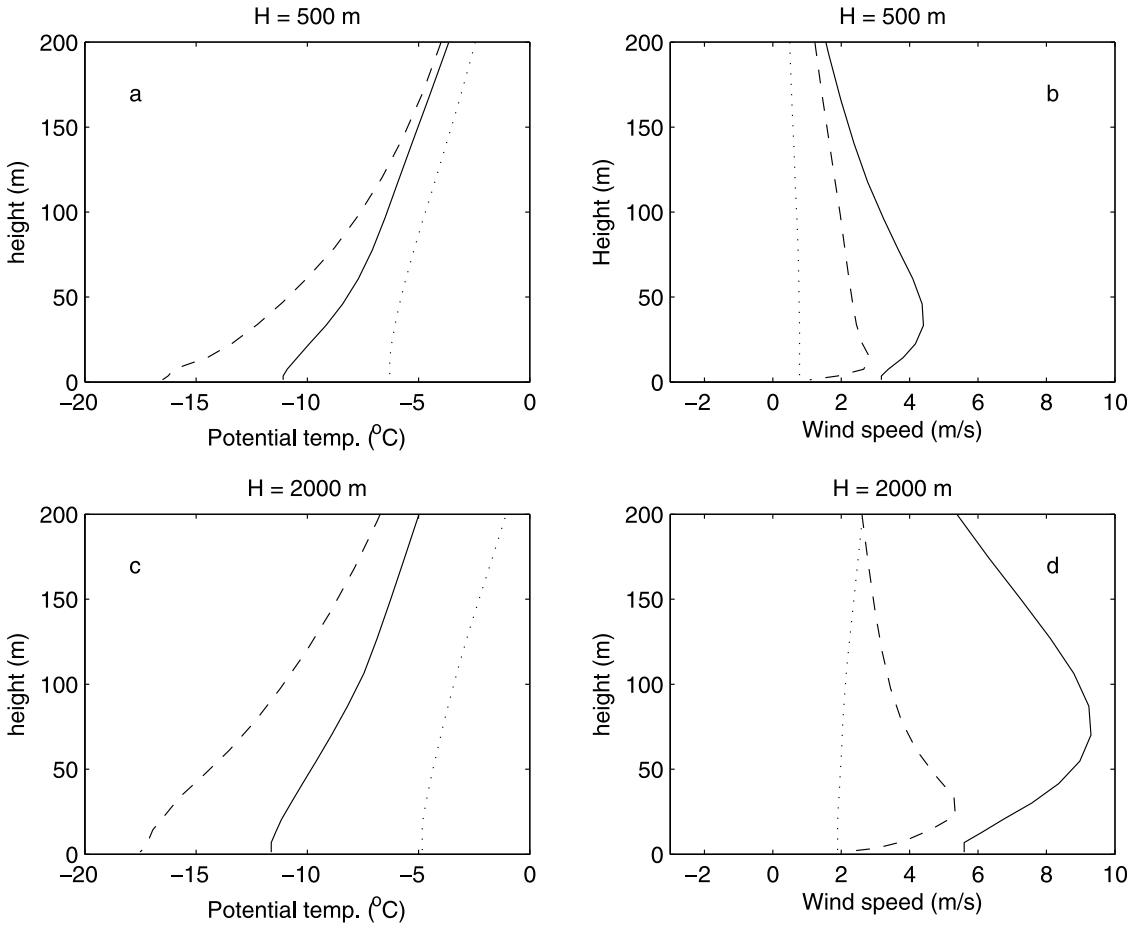

Figure 4. Vertical profiles of (a, c) potential temperature and (b, d) horizontal and vertical wind speeds in the middle of the sea ice zone (dashed lines), the slope (solid lines), and the high plateau (dotted lines) in experiments H2 (slope height of 500 m) and H5 (slope height of 2000 m).

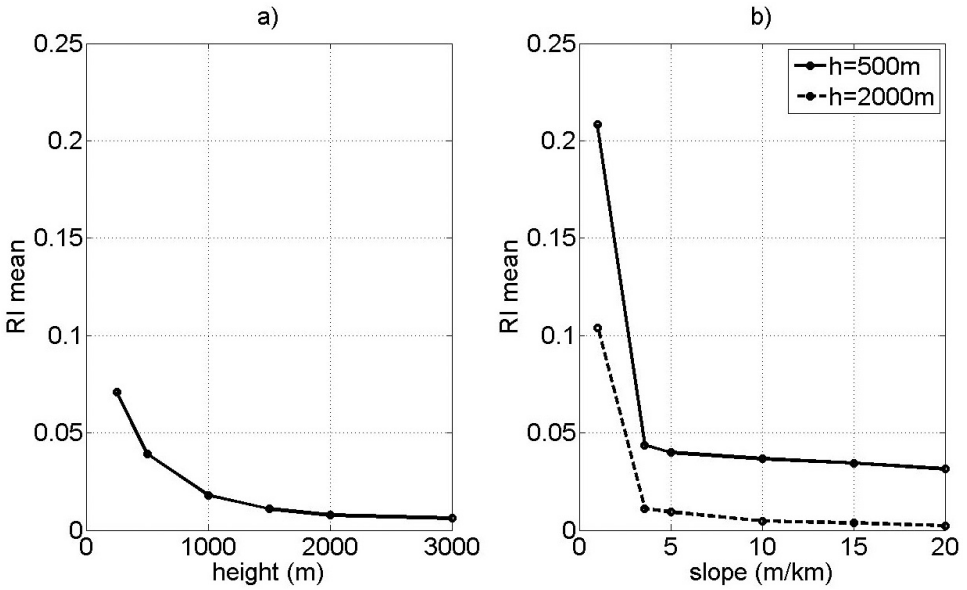

Figure 5. Ri_{2m} averaged over the slope for (a) various slope heights and (b) various slope angles.

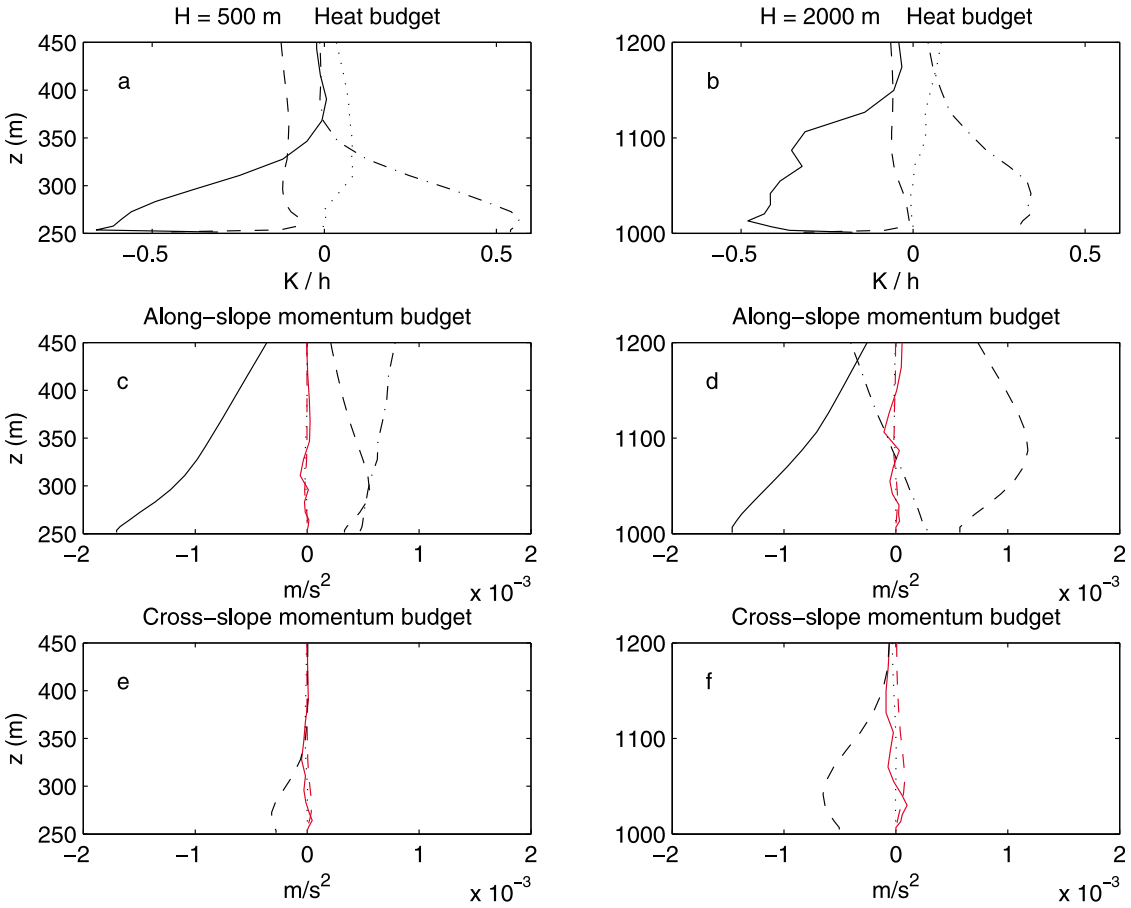

Figure 6. Vertical profiles of the terms in the equations of (a, b) heat budget (convergence of sensible heat flux (solid lines), convergence of net radiative flux (dashed lines), horizontal advection (dot–dashed lines), and vertical advection (dotted lines)) and (c, d) along-slope and (e, f) cross-slope momentum budget (buoyancy (solid lines), thermal wind (dot–dashed lines), Coriolis term (dashed lines), convergence of turbulent momentum flux (red solid lines), vertical advection (dotted lines), and horizontal advection (red dashed lines)). The terms are presented at the middle of the slope for experiments H2 (slope height of 500 m) and H5 (slope height of 2000 m), as in Figure 4.

$$\frac{\partial v}{\partial t} = -u\frac{\partial v}{\partial x} - w\frac{\partial v}{\partial z} - fu - \frac{1}{\rho}\frac{\partial \tau_y}{\partial z}, \tag{4}$$

$$\frac{\partial \theta}{\partial t} = -u\frac{\partial \theta}{\partial x} - w\frac{\partial \theta}{\partial z} - \frac{1}{\rho c_p}\frac{\partial F_R}{\partial z} - \frac{1}{\rho c_p}\frac{\partial F_H}{\partial z}, \tag{5}$$

where u, v, and w denote the three orthogonal wind components, f is the Coriolis parameter, g is the acceleration that is due to gravity, α is the slope angle, τ is the turbulent momentum flux, F_R is the net radiation, F_H is the turbulent flux of sensible heat, ρ is air density, and c_p is the specific heat. Diabatic heating/cooling due to condensation/evaporation is negligible in the cases simulated. Equation (3) is written in coordinates following the slope. Hence, the pressure gradient force is the sum of the fourth and fifth terms on the right-hand side. The fourth term represents the effect of buoyancy; $\Delta\theta$ is the potential temperature deficit in the katabatic layer and θ_0 is the reference potential temperature above the katabatic layer (at height h, following *Yu et al.* [2005], h is defined as the height at which the vertical gradient of the potential temperature falls below 0.01 K m^{-1}). The fifth term represents the thermal wind effect, where $\overline{\Delta\theta}(z)$ is the average potential temperature deficit between heights z and h [*Mahrt*, 1982]. In the case of no slope, this term becomes the classical thermal wind term driving sea breeze–type mesoscale circulations due to differential surface heating.

[16] Figure 6 presents the vertical profiles of the terms in (3)–(5) in the middle of the slope, with experiments H2 (slope height 500 m) and H5 (2000 m) as examples. The vertical profiles of the momentum budget equations demonstrate that the buoyancy force tends to accelerate the downslope wind (decelerate u wind component). When the slope height is small (500 m), the thermal wind effect opposes the buoyancy force. The thermal wind is generated by the accumulation of cold air over the sea ice and lower parts of the slope. It is, however, close to zero when the slope height is large (2000 m), and upward of the height of 70 m it starts to support the katabatic flow (see section 4.2). The Coriolis effect dominates the cross-slope momentum equation, resulting in an inertial oscillation with an amplitude of 0.5 m s^{-1} in the v wind component (see section 5.1). The katabatic layer is heated by horizontal and vertical heat

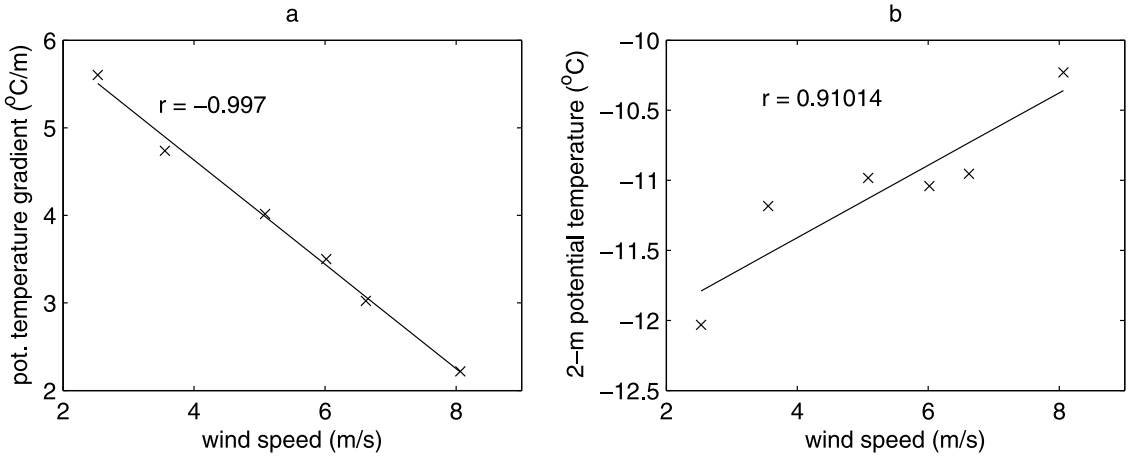

Figure 7. Effect of the wind speed on the vertical gradient of (a) θ and (b) θ_{2m}. Both the wind speed and the vertical gradient of θ are averaged over the slope and in the layer from the snow surface to the height of 100 m.

advection and cooled by the divergence of the sensible heat flux and, less strongly, by the divergence of the net longwave radiation (Figure 6). This is in accordance with the profiles of potential temperature and wind speed (Figure 4).

[17] Comparing experiments H1–H6 with different slope heights, we see that the enhanced turbulent mixing under stronger winds over higher slopes (Figure 3) decreases the vertical gradient of potential temperature (Figure 7a) and increases θ_{2m} (Figure 7b). The latter does not contradict the role of the divergence of sensible heat flux in cooling the katabatic layer (Figure 6): Turbulence transports heat from air to the snow surface; the stronger the wind, the larger the transport. Under a strong wind, however, the transport takes place in a thicker layer and the cooling at the height of 2 m remains smaller. In all cases, the turbulent and radiative cooling is approximately balanced by advective heating.

[18] Considering T_{2m} (Figure 3b), effects of adiabatic warming by the downslope flow are included. When the slope height is small (H below 1 km), the adiabatic warming is not enough to balance the downslope decrease of θ_{2m}, and T_{2m} accordingly decreases along the slope fall line. The slope height of 1000 m represents a transition zone where T_{2m} remains nearly constant along the slope fall line (Figure 3b), and for slope heights of 1500 m and more, the temperature along the slope fall line increases toward the sea ice.

[19] To find the relative importance of the surface inversion over the flat sea ice for T_{2m} (mechanism 3 above), we carried out an additional experiment (H0), which was otherwise similar to H1–H6 except that the slope height was set to zero. The resulting surface-based inversion layer was about 260 m thick with a temperature increase of 12.5°C. Hence, in experiment H1, although mechanisms 1–3 all contribute, mechanism 3 alone would have resulted in the downslope decrease in T_{2m}, whereas in experiment H2 mechanisms 1 and 2 were also necessary for the downslope decrease. In H1, T_{2m} decreases downslope by 4°C, which is still much less than the inversion strength in H0. Hence, even over a small slope of 250 m, the weak katabatic wind has a strong effect in reducing the inversion strength on the slope. Over the sea ice, the inversion strength in H1 (11°C) is close to that in H0. The inversion depth in H1 is 400 m at the coastline; the high value (compared to 260 m in H0) demonstrates the importance of mechanism 1, which via the thermal wind effect provides a negative feedback to the downslope flow.

4. The Effect of Slope Angle

[20] Results of section 3 indicated that the response in T_{2m} is basically different for low and high slopes. Hence, the slope height H is now fixed either to the low 500 m (experiments S1.1–S1.6) or the high 2000 m (experiments S2.1–S2.6), and the slope aspect ratio is varied from the low 1 m km^{-1} to the high 20 m km^{-1} (corresponding to the slope angles of 0.06°, 0.2°, 0.3°, 0.6°, 0.86°, and 1.15°, respectively). The simulations are initialized as in section 3. The results are shown in Figures 8 and 9.

4.1. Slope Height of 500 m

[21] Figure 8 indicates that the lowest aspect ratio of 1 m km^{-1} is too weak to induce coherent katabatic winds along a low slope. For increasing slope angles, the downslope wind component u increases in strength (u − 2 … −4 m s^{-1}, Figure 8c) with the maximum transverse left-turned component (v) remaining rather the same, about −2.5 m s^{-1} (Figure 8d). In the lower parts of the slope, the thermal wind opposes the katabatic flow. The effect was largest for small slope angles with the weakest winds, which is analogous to the results in section 3. With the slope height of 500 m, θ_{2m} increases with the slope angle, increasing from 1 to 20 m km^{-1} (Figure 8a). Analogous to experiments H1–H6, this is due to the stronger winds and, accordingly, the weaker heat flux divergences at the height of 2 m.

[22] The θ_{2m} had already decreased on the plateau toward the start of the slope (Figure 8a). This is due to the increase of the wind speed from zero to a maximum of 4 m s^{-1}, which results in an increasing downward sensible heat flux. Over the plateau 100 km from the slope, the stratification is very stable, with the snow surface thermally almost decoupled from the air. Hence, at the height of 2 m there is convergence of the downward sensible heat flux, which heats the air by 0.8 K h^{-1}, but the convergence decreases

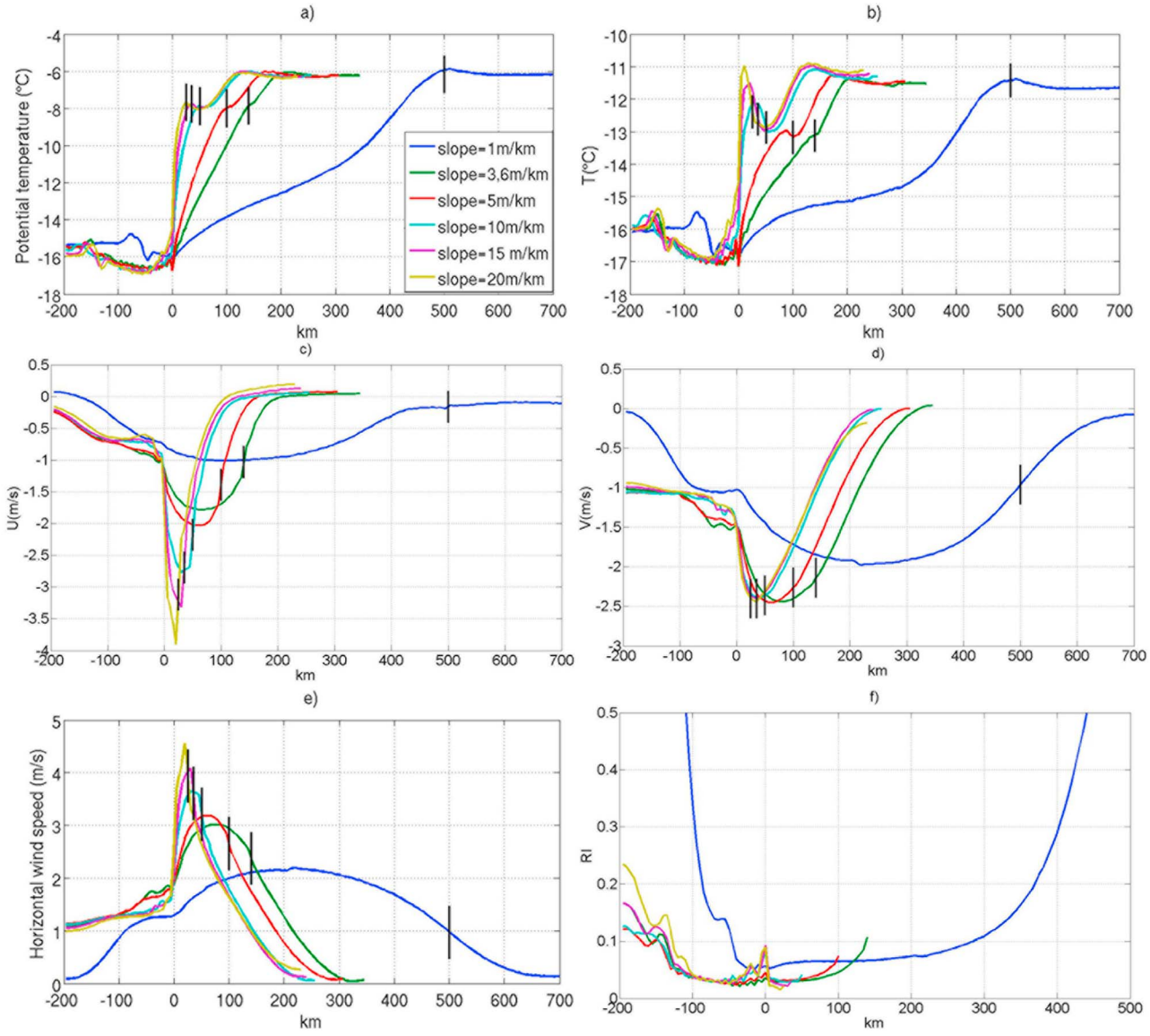

Figure 8. As in Figure 3 but for simulation results when the slope angle varies and the slope height is 500 m.

to 0.2 K h^{-1} by the beginning of the slope. Hence, θ_{2m} decreases toward the beginning of the slope (but the snow surface temperature increases).

[23] With all slope angles ranging from 1 to 20 m km^{-1}, θ_{2m} and T_{2m} decrease from the high plateau toward the sea ice (Figures 8a and 8b). The decrease of T_{2m} is, however, not monotonous: In the upper parts of the steeper slopes (aspect ratio of at least 0.005) the convergence of the sensible heat flux is slightly positive (0.2 K h^{-1}) and, together with adiabatic warming, generates a downslope increase in T_{2m} in the upper part of the slope (Figure 8b; this feature is slightly detectable also in the distribution of θ_{2m} over the steeper slopes in Figure 8a). Further downslope the convergence changes to negative (−1.5 K h^{-1}), which results in a rapid decrease in T_{2m}. Over the sea ice T_{2m} shows very little dependence on the slope angle, implying the weakening of the katabatic flow.

[24] Excluding the gentlest slope (1 m km^{-1}), Ri_{2m} mostly stays below 0.1 over the slope (Figure 8f). The conditions are most stable over the high plateau (as in Figure 4a for experiment S2), over the northern half of the sea ice zone, in the upper part of the slope, and, for the steepest slopes, on the coast. Averaged over the length of the slope, Ri_{2m} decreases as the slope angle increases from 1 to 20 m km^{-1} (Figure 5b).

4.2. Slope Height of 2000 m

[25] Figure 9 shows that the longer and higher 2 km slope triggers a stronger downslope wind component for each aspect ratio than for the low 0.5 km slope of Figure 8. The steepest (aspect ratios of 0.015–0.020) 2 km slopes maintain

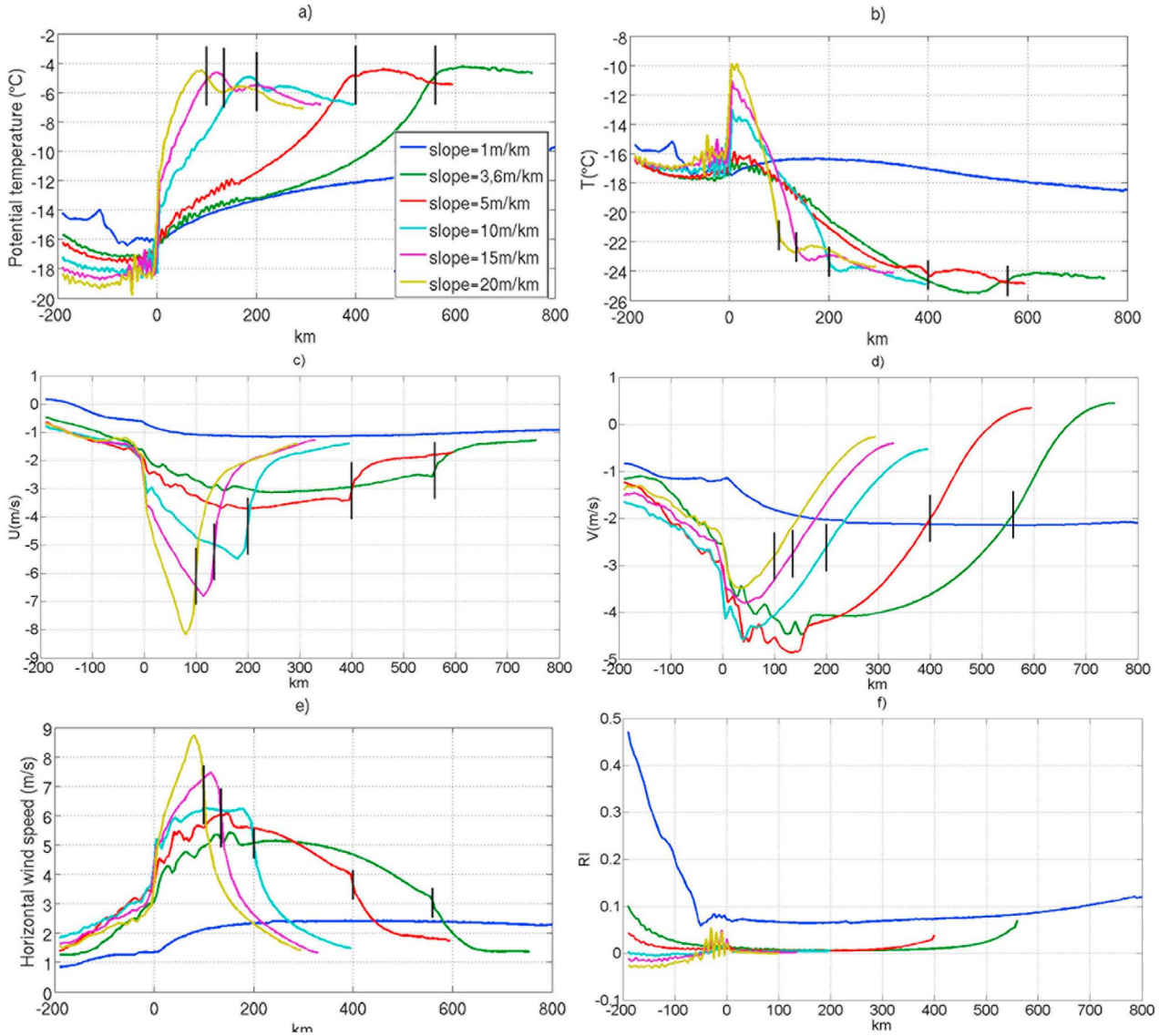

Figure 9. As in Figure 3 but for simulation results when the slope angle varies and the slope height is 2000 m. The slope with smallest angle is only partly shown because of its substantial x dimension.

a maximum 2 m wind speed of 7.5–9 m s^{-1} from 156° in Figure 9, not much unlike the observed 10 m mean wintertime winds of 10–12 m s^{-1} from 130° to 150° in Dumont d'Urville. Even the 0.0036 slope sustains a katabatic wind of 5 m s^{-1} from 124° (Figure 9). As in the case of the 500 m slope, these katabatic winds extend somewhat upstream over the cold high plateau.

[26] Now with the high slope, the thermal wind effect is insignificant in the lower parts of the slope. Over the high plateau, however, weak katabatic winds start already some 50 km south of the slope. This is due to the thermal wind effect near the top of the slope. The snow surface over the plateau cools radiatively, also cooling the near-surface air into a strong surface inversion. Air over the slope at the same height above sea level is farther from the local snow surface and therefore remains warmer (in the case of the steepest slope, the horizontal temperature gradient reached 8.5°C/20 km). This results in a pressure gradient generating the wind over the plateau. The effect of this upper thermal wind was present in all simulations (Figures 3, 8, and 6d), but it is most pronounced here with a high and steep slope (Figure 9).

[27] As in the previous experiments, θ_{2m} decreases along the fall line toward the foot of the slope with all slope angles. Here, for all slope angles between 1 and 20 m km^{-1}, because of the strong adiabatic and turbulent effects, T_{2m} increases monotonically down the fall line, almost until the foot of the slope (Figure 9b). As in the case of the 500 m slope, near the foot of the slope the near-surface temperature decreases suddenly, just before the flow arrives to the sea ice. The T_{2m} decrease is largest (approximately 6°C) in the case of the steepest slope. The simultaneously decreasing wind speed (Figure 9e) and increasing stratification (Figure 9f) are evident. These suggest the presence of a hydraulic jump (also called as a katabatic jump). Although a hydrostatic model cannot reproduce its detailed structure, we calculated the

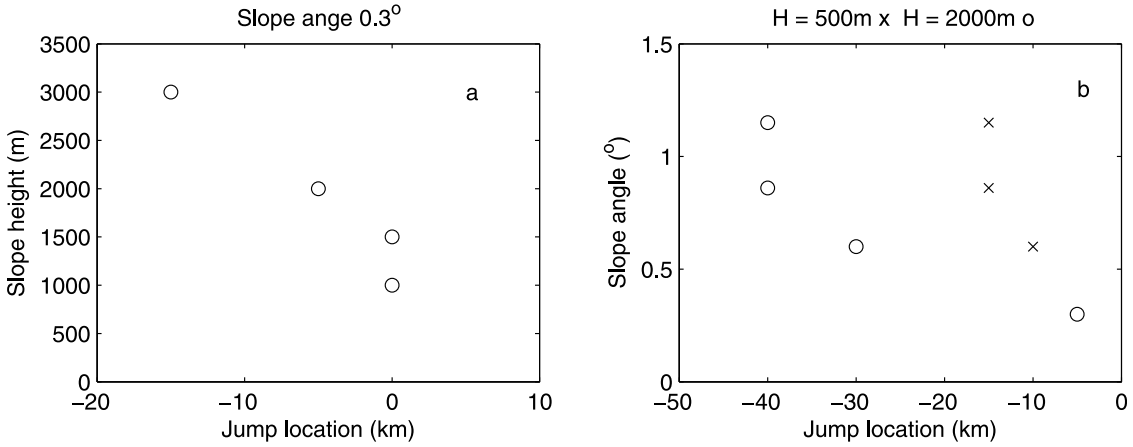

Figure 10. Location of the katabatic jump in model experiments with (a) varying slope height and (b) varying slope angle.

mean Froude number (*Fr*) in the katabatic layer [*Yu et al.*, 2005]:

$$Fr = \frac{\theta_h V_m^2}{gh(\theta_m - \theta_h)}, \tag{6}$$

where V_m and θ_m are the mean wind speed and potential temperature, respectively, in the katabatic layer of height h, and θ_h is θ at h. Experiments H3–H6, S1.4–S1.6, and S2.3–S2.6 indicated a location where *Fr* dropped below 1, suggesting a change from a supercritical to a subcritical flow. The jump was located either at the foot of the slope or 5–40 km further downstream (Figure 10): The stronger the katabatic wind speed (high or steep slope), the farther downstream the jump was located. The hydraulic jump was collocated with the steepest decrease in the mean wind speed in the katabatic layer, which was downstream from that of the 2 m wind speed (Figures 3 and 8–10).

5. Comparison Against Previous Studies

5.1. Katabatic Wind Dynamics

[28] On the basis of scale analysis, *Mahrt* [1982] argued that with a small Froude number, the buoyancy term may be approximately balanced by the thermal wind term because of increasing flow depth and temperature deficit in the downslope direction. This corresponds to our results for the weaker katabatic winds along smaller and less steep slopes. Also, the model simulations of *Yu and Cai* [2006] showed that the thermal wind effect related to the cold-air pool at the lower parts of the slope is important in decelerating the downslope flow. *Mahrt* [1982] also suggested a negligible role of momentum advection in conditions with $Fr\, h/H \ll 1$, which is in agreement with our results and the climate model simulations by *van den Broeke and van Lipzig* [2003]. Further, we found the vertical convergence of momentum flux as a minor term in the budget equation, which also agrees with *Mahrt* [1982] but contradicts the classical theory of *Prandtl* [1942], in which the buoyancy force is balanced by the diffusion of momentum (in a laminar flow).

[29] We observed that the downslope flow speed increased with increasing slope heights and slope angles up to 1.15°. This is in agreement with the scale analysis by *Mahrt* [1982] and modeling experiments on katabatic winds in the Antarctic [*van den Broeke and van Lipzig*, 2003; *Davis and McNider*, 1997] and Svalbard in the Arctic [*Livik*, 2011]. This result, however, is not necessarily valid for very steep slopes: The direct numerical simulation (DNS) experiments by *Fedorovich and Shapiro* [2009] showed that the downslope wind speed was stronger for a slope angle of 30° than for a slope angle of 60°. For very large slope angles with a thin katabatic layer, the effects of the thermal wind are negligible, which partly explains the difference between our results and those of *Fedorovich and Shapiro* [2009]. Another aspect is that *Fedorovich and Shapiro* [2009] applied infinite x and y axes in the DNS. Such a model configuration lacks the flat sea ice (or ice shelf) at the foot of the slope. Accordingly, a cold-air pool is not generated on the flat surface, and the thermal wind effect would be dramatically underestimated even for small slope angles.

[30] The cross-slope wind component in the 2-D model was not entirely in a steady state after 48 h integration (Figures 6e and 6f). This has been the case also in previous studies: *Stiperski et al.* [2007], who included the Coriolis force in the *Prandtl* [1942] model, did not reach a true steady state for the cross-slope component, and the DNS results of *Fedorovich and Shapiro* [2009] displayed persistent low-frequency oscillatory motions with a frequency of $N \sin \alpha$, where N is the Brunt-Väisälä frequency and α is the slope angle.

[31] At Dumont d'Urville, *Argentini et al.* [1996] observed katabatic wind core heights of 100 to 200 m. Dumont d'Urville is located on an island almost 2 km from the slope. On the coast, the slope is steep, with an aspect ratio of about 15 m km^{-1}, and reaches up to 1800 m. In the almost corresponding experiment S2.5, at 0–5 km from the foot of the slope we simulated a core height of 50 m, which is a clear underestimation. On the other hand, the simulations presented in section 2.2, with validation against observations of T_{2m} and 10 m wind at Dumont d'Urville and Mawson, resembled experiment S2.5 and added confidence in its results on the relationship of near-surface wind and temperature.

[32] Our model output provided a possibility for a quantitative comparison against *Ball*'s [1960] analytic two-layer model. The two layers are characterized by constant

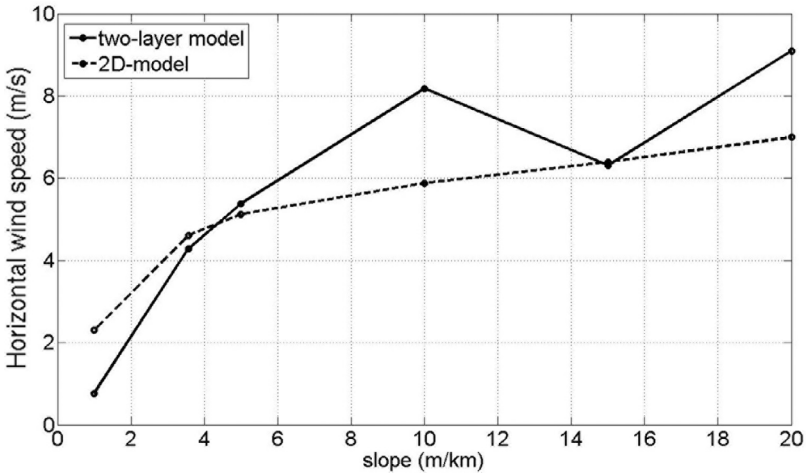

Figure 11. The near-surface wind speeds modeled by the analytic two-layer model and the 2-D model.

potential temperatures, and the lower layer has a certain depth D, whereas the upper layer is infinite in the vertical. The surface slopes uniformly with angle α and is infinitely long. It is assumed that the flow in the upper layer is geostrophic and there is no friction between the two layers. In the near-surface layer the wind speed is constant with height and is governed by the slope effect, the given geostrophic wind (if any), and the linear surface drag, leading to the speed and direction of the steady state katabatic flow being analytic functions of the θ difference between the layers, D, V_g, and α. On the basis of the results produced by the 2-D model for variable α (Figure 8), the depth D of the near-surface layer was defined to be the height of the maximum near-surface wind speed multiplied by 2, and θ of the lower layer was set to the mean of the 2-D model's θ over the slope in this layer. For the upper layer, θ was defined to be the mean potential temperature over the slope at height D. Note that no wind information is provided for the two-layer model application directly (except that $V_g = 0$).

[33] The two-layer model's wind speed, calculated as described above from the 2-D model temperature output for variable α, and the 2-D model's actual wind speed are in good agreement (Figure 11). Both models generate the weakest wind over the gentlest slope. The two-layer analytic approach produces slightly stronger wind speeds than the 2-D model in the case of the steepest slope angles. Unfortunately, Ball's two-layer model uses fixed temperatures and so gives no information about the horizontal θ_{2m} and T_{2m} distributions.

5.2. Effects on Air Temperature

[34] The 2-D model results allow comparison against observations from various topographic conditions around Antarctica. Several studies have addressed the effect of katabatic winds on the temporal change in the air temperature [*Ohata et al.*, 1982; *Périard and Pettré*, 1993; *Streten*, 1990; *Argentini et al.*, 2001; *van As and van den Broeke*, 2007], but we have to focus on a comparison against studies that report spatial differences in the air temperature during katabatic wind events. According to *Hogan* [1997] and *van den Broeke and van Lipzig* [2003], the lowest potential temperatures in the Antarctica occur on the high plateau and on the Ross and Ronne Ice Shelves, the latter being due to the accumulation of cold air carried by katabatic winds. The occurrence of very low potential temperatures also on the high plateau demonstrates that accumulation is not the only reason: The stronger stratification over flat regions with weak wind also contributes to the low potential temperatures. Our results are in agreement with *Hogan* [1997] and *van den Broeke and van Lipzig* [2003]. Under particularly strong wind events, three-dimensional (3-D) nonstationary and nonkatabatic effects may, however, generate wind-temperature relationships that differ a lot from the climatology: *Breckenridge et al.* [1993] showed that during a wintertime strong wind event the potential temperature on the Ross Ice Shelf was 15°C higher than on the east Antarctic plateau.

[35] *Parish and Bromwich* [1989] presented two cases of aircraft observations on katabatic winds near Terra Nova Bay, east Antarctica. As averaged over the 310 km slope at the flight level of 170 m, in both cases the potential temperature decreased and the true air temperature increased down the slope. The slope height was 2150 m, and the aspect ratio was 7 m km^{-1} (estimated from Figure 3 in Parish and Bromwich). Although their study environment was complex, with 3-D effects of localized topographic channeling, the results for the large-scale behavior of both true and potential temperatures are in agreement with our simulations for the slope height of 2000 m. In locations of the strongest katabatic winds, warming of the surface due to enhanced turbulent mixing dominated, seen as warm signatures in the infrared satellite images of *Parish and Bromwich* [1989].

[36] The Polar MM5 model experiments of *Monaghan et al.* [2005] resulted in an increase of T_{2m} down the slope in the coastal region west of McMurdo. The slope height was more than 1500 m, and the aspect ratio was approximately 17 m km^{-1}. Accordingly, the results are in agreement with ours.

[37] *Zwally and Fiegles* [1994] analyzed the surface melting on the Antarctic ice shelves and in the margins of the ice sheet on the basis of satellite passive microwave data. They concluded that some melt patterns were related to

katabatic wind heating of the surface. These were observed (1) on the northern part of the Amery Ice Shelf, Kreitser Glacier and on the ice sheet up to about 1000 m elevation, and (2) on the lower Lambert Glacier down to the grounding line. These are regions of steep slopes of roughly 10 m km^{-1} up to the height of 2000 m. According to our 2-D model results, the temperature maximum should indeed occur in the lower parts of the slope.

[38] In most of our model experiments θ_{2m} had already decreased on the plateau toward the start of the slope (Figures 3 and 8). This was due to the increase of the wind speed from zero to a maximum of 4 m s^{-1}, which resulted in an increasing downward sensible heat flux from the height of 2 m to the snow surface. This is in accordance with *Lüpkes et al.* [2008], who observed that the lowest near-surface air temperatures over the Arctic sea ice do not occur during calm conditions but under a wind of 4 m s^{-1}.

6. Conclusions

[39] Katabatic winds were simulated without basic flow above various slopes in Antarctic wintertime conditions. In all cases, θ_{2m} decreased along the fall line toward the foot of the slope. We identified three mechanisms for this: (1) the katabatic wind resulted in accumulation of radiatively cooled near-surface air over the sea ice and over the lower parts of the slope; (2) over the flat and calm sea ice zone, the stratification was stronger, resulting in lower near-surface temperatures; and (3) the shallower slopes were within the strong surface inversion from over the sea ice. With the slope aspect ratio fixed at 5 m km^{-1} and a slope height below 1000 m, T_{2m} also decreased down the slope, but for slope heights of 1500 m and more, T_{2m} increased down the slope. This was because of the stronger adiabatic warming and, because of stronger winds, enhanced downward flux of sensible heat, the latter reducing the downslope decrease of θ_{2m}. The katabatic layer was heated by horizontal and vertical advection and cooled by the divergence of sensible heat flux and net longwave flux. Under a strong wind, the turbulent transport of heat from the air to snow surface took place in a thicker layer. Hence, the cooling at the height of 2 m was smaller.

[40] With a small slope height of 500 m, for all slope angles ranging from 1 to 20 m km^{-1}, T_{2m} decreased along the fall line but not monotonically: In the steeper slopes the adiabatic warming and warming due to turbulent mixing together dominated over the cooling factors, seen as a downslope increase in T_{2m} in the upper part of the slope. With a large slope height of 2000 m, for all slope angles between 1 and 20 m km^{-1}, T_{2m} increased monotonically instead down the fall line. The effects of slope height and angle on the along-slope distribution of θ_{2m} and T_{2m} agreed reasonably well with several observations with different topographies around Antarctica.

[41] According to our knowledge, previous studies have not distinguished between the opposite effects of the thermal wind along the slope. Close to the foot of the slope, where the colder air lays in the downstream direction (over the sea ice), the thermal wind opposes the katabatic flow. This thermal wind effect was strongest when the slope was low with a small aspect ratio, as already shown by *Mahrt* [1982]. Over the high plateau, the snow surface was strongly cooled by negative net radiation, and stable stratification was established in the near-surface air. Over the upper parts of the slope, the air at the same altitude above sea level thus remained warmer, being located in the warm inversion layer. Hence, the thermal wind here supports the katabatic flow and generates a flow toward the slope already over the plateau. This thermal wind effect was strongest when the slope was steep and high. With a steeper slope, the horizontal temperature gradient was affected by warmer inversion-layer air over the slope, higher above the local cold surface. With a high slope the inversion based on the sea ice did not affect the temperatures near the top of the slope. Thus the thermal wind effects on the wind field over Antarctica are rather complex and deserve more studies applying observations and 3-D models.

[42] We finally note that in our simulations the surface below the slope was thick, snow-covered sea ice with 100% ice concentration. With negligible conductive heat flux through the sea ice and snow, the results also well represent conditions on a flat ice shelf below the slope. In the case of coastal polynyas or leads in the sea ice zone, however, the temperature and wind conditions would have been affected [*Heinemann*, 2003; *Savijärvi*, 2011].

[43] **Acknowledgments.** The study was supported by the Academy of Finland (contracts 128533 and 128799). The ECMWF is acknowledged for providing model analyses. We thank the anonymous reviewers for their valuable comments.

References

Alpert, P., A. Cohen, E. Doron, and J. Neumann (1982), A model simulation of the summer circulation from the eastern Mediterranean past Lake Kinneret in the Jordan Valley, *Mon. Weather Rev.*, *110*, 994–1006, doi:10.1175/1520-0493(1982)110<0994:AMSOTS>2.0.CO;2.

Argentini, S., G. Mastrantonio, A. Viola, P. Pettre, and G. Dargaud (1996), Sodar performance and preliminary results after one year of measurements at Adelie Land coast, east Antarctica, *Boundary Layer Meteorol.*, *81*, 75–103, doi:10.1007/BF00119401.

Argentini, S., I. V. Petenko, G. Mastrantonio, V. A. Bezverkhnii, and A. P. Viola (2001), Spectral characteristics of east Antarctica meteorological parameters during 1994, *J. Geophys. Res.*, *106*, 12,463–12,476, doi:10.1029/2001JD900112.

Ball, F. K. (1960), Winds on the ice slopes of Antarctica, in *Antarctic Meteorology*, pp. 9–16, Pergamon, London.

Barry, R. G. (2008), *Mountain Weather and Climate*, 506 pp., Cambridge Univ. Press, Cambridge, U. K., doi:10.1017/CBO9780511754753.

Breckenridge, C. J., U. Radok, C. R. Stearns, and D. H. Bromwich (1993), Katabatic winds along the Transantarctic Mountains, in *Antarctic Meteorology and Climatology: Studies Based on Automatic Weather Stations*, *Antarct. Res. Ser.*, vol. 61, edited by D. H. Bromwich and C. R. Stearns, pp. 69–92, AGU, Washington, D.C.

Bromwich, D. H., J. F. Carrasco, and C. R. Stearns (1992), Satellite observations of katabatic-wind propagation for great distances across the Ross Ice Shelf, *Mon. Weather Rev.*, *120*, 1940–1949, doi:10.1175/1520-0493(1992)120<1940:SOOKWP>2.0.CO;2.

Davis, A. M. J., and R. T. McNider (1997), The development of Antarctic katabatic winds and implications for the coastal ocean, *J. Atmos. Sci.*, *54*, 1248–1261, doi:10.1175/1520-0469(1997)054<1248:TDOAKW>2.0.CO;2.

Dee, D. P., et al. (2011), The ERA-Interim Reanalysis: Configuration and performance of the data assimilation system, *Q. J. R. Meteorol. Soc.*, *137*, 553–597, doi:10.1002/qj.828.

Defant, A. (1933), Der abfluss schwerer Luftmassen auf geneigten boden, nebst einigen bemerkungen zur theorie stationärer luftstrome, *Sitz. Berichte Preuss. Akad. Wiss.*, *18*. 624–635.

Fedorovich, E., and A. Shapiro (2009), Structure of numerically simulated katabatic and anabatic flows along steep slopes, *Acta Geophys.*, *57*, 981–1010, doi:10.2478/s11600-009-0027-4.

Gahmberg, M., H. Savijärvi, and M. Leskinen (2010), The influence of synoptic scale flow on sea breeze induced surface winds and calm zones, *Tellus, Ser. A*, *62*, 209–217, doi:10.1111/j.1600-0870.2009.00423.x.

Heinemann, G. (2003), Forcing and feedback mechanisms between the katabatic wind and sea ice in the coastal areas of polar ice sheets, *J. Atmos. Ocean Sci.*, *9*, 169–201.

Hogan, A. (1997), A synthesis of warm air advection to the South Polar Plateau, *J. Geophys. Res.*, *102*, 14,009–14,020, doi:10.1029/97JD00282.

King, J. C., and J. Turner (1997), *Antarctic Meteorology and Climatology*, 409 pp., Cambridge Univ. Press, U. K., doi:10.1017/CBO9780511524967.

Kottmeier, C. (1986), Shallow gravity flows over the Ekstrom Ice Shelf, *Boundary Layer Meteorol.*, *35*, 1–20, doi:10.1007/BF00117299.

Livik, G. (2011), An observational and numerical study of local winds in Kongsfjorden, Spitsbergen, M.S. thesis, 110 pp., Geophys. Inst., Univ. of Bergen, Bergen, Norway.

Lüpkes, C., T. Vihma, G. Birnbaum, and U. Wacker (2008), Influence of leads in sea ice on the temperature of the atmospheric boundary layer during polar night, *Geophys. Res. Lett.*, *35*, L03805, doi:10.1029/2007GL032461.

Mahrt, L. (1982), Momentum balance of gravity flows, *J. Atmos. Sci.*, *39*, 2701–2711, doi:10.1175/1520-0469(1982)039<2701:MBOGF>2.0.CO;2.

Monaghan, A. J., D. H. Bromwich, J. G. Powers, and K. W. Manning (2005), The climate of the McMurdo, Antarctica, region as represented by one year of forecasts from the Antarctic Mesoscale Prediction System, *J. Climatol.*, *18*, 1174–1189, doi:10.1175/JCLI3336.1.

Monti, P., H. J. S. Fernando, M. Princevac, W. C. Chan, T. A. Kowalewski, and E. R. Pardyjak (2002), Observations of flow and turbulence in the nocturnal boundary layer over slope, *J. Atmos. Sci.*, *59*, 2513–2534, doi:10.1175/1520-0469(2002)059<2513:OOFATI>2.0.CO;2.

Ohata, T., M. Wada, and S. Kawaguchi (1982), Stability of the air layer near the snow surface at Mizuho Station, Antarctica, in *Memoirs, Special Issue*, vol. 24, pp. 43–45, Natl. Inst. of Polar Res., Tokyo, Japan.

Parish, T. R., and D. H. Bromwich (1989), Instrumented aircraft observations of the katabatic wind regime near Terra Nova Bay, *Mon. Weather Rev.*, *117*, 1570–1585, doi:10.1175/1520-0493(1989)117<1570:IAOOTK>2.0.CO;2.

Parish, T. R., and G. Wendler (1991), The katabatic wind regime at Adelie Land, Antarctica, *Int. J. Climatol.*, *11*, 97–107, doi:10.1002/joc.3370110108.

Périard, C., and P. Pettré (1993), Some aspects of the climatology of Dumont d'Urville, Ade1ie Land, Antarctica, *Int. J. Climatol.*, *13*, 313–327, doi:10.1002/joc.3370130307.

Poulos, G. S., J. E. Bossert, T. B. McKee, and R. A. Pielke (2007), The interaction of katabatic flow and mountain waves. Part II: Case study analysis and conceptual model, *J. Atmos. Sci.*, *64*, 1857–1879, doi:10.1175/JAS3926.1.

Prandtl, L. (1942), *Führer Durch die Strömungslehre*, 382 pp., F. Vieweg & Sohn, Braunschweig, Germany.

Prandtl, L. (1952), *Essentials of Fluid Dynamics: With Applications to Hydraulics, Aeronautics, Meteorology and Other Subjects*, translated from German by W. M. Deans, 452 pp., Blackie, London.

Reuder, J., et al. (2011), FLOHOF 2007: An overview of the mesoscale meteorological field campaign at Hofsjökull, central Iceland, *Meteorol. Atmos. Phys.*, doi:10.1007/s00703-010-0118-4, in press.

Savijärvi, H. (2009), Stable boundary layer: Parametrizations for local and larger scales, *Q. J. R. Meteorol. Soc.*, *135*, 914–921, doi:10.1002/qj.423.

Savijärvi, H. (2011), Antarctic local wind dynamics and polynya effects on the Adelie Land coast, *Q. J. R. Meteorol. Soc.*, doi:10.1002/qj.874.

Savijärvi, H., S. Niemelä, and P. Tisler (2005), Coastal winds and low level jets: Simulations for sea gulfs, *Q. J. R. Meteorol. Soc.*, *131*, 625–637, doi:10.1256/qj.03.177.

Stiperski, I., I. Kavcic, B. Grisogono, and D. R. Durran (2007), Including Coriolis effects in the Prandtl model for katabatic flow, *Q. J. R. Meteorol. Soc.*, *133*, 101–106, doi:10.1002/qj.19.

Streten, N. A. (1990), A review of the climate of Mawson—A representative strong wind site in east Antarctica, *Antarct. Sci.*, *2*, 79–89, doi:10.1017/S0954102090000098.

Turner, J., and S. Pendlebury (Eds.) (2004), *The International Antarctic Weather Forecasting Handbook*, 685 pp., Br. Antarct. Surv., Cambridge, U. K.

van As, D., and M. R. van den Broeke (2007), Causes of variability in the summertime Antarctic boundary-layer climate, *Int. J. Climatol.*, *27*, 1735–1751, doi:10.1002/joc.1488.

van den Broeke, M. R., and N. P. M. van Lipzig (2003), Factors controlling the near-surface wind field in Antarctica, *Mon. Weather Rev.*, *131*, 733–743, doi:10.1175/1520-0493(2003)131<0733:FCTNSW>2.0.CO;2.

Vihma, T., and B. Brümmer (2002), Observations and modelling of on-ice and off-ice flows in the northern Baltic Sea, *Boundary Layer Meteorol.*, *103*, 1–27, doi:10.1023/A:1014566530774.

Vihma, T., J. Hartmann, and C. Lüpkes (2003), A case study of an on-ice air flow over the Arctic marginal sea ice zone, *Boundary Layer Meteorol.*, *107*(1), 189–217, doi:10.1023/A:1021599601948.

Vihma, T., C. Lüpkes, J. Hartmann, and H. Savijärvi (2005), Observations and modelling of cold-air advection over Arctic sea ice in winter, *Boundary Layer Meteorol.*, *117*, 275–300, doi:10.1007/s10546-004-6005-0.

Yu, Y., and X. Cai (2006), Structure and dynamics of katabatic flow jumps: Idealized simulations, *Boundary Layer Meteorol.*, *118*, 527–555, doi:10.1007/s10546-005-6433-5.

Yu, Y., X. Cai, J. C. King, and I. A. Renfrew (2005), Numerical simulations of katabatic jumps in Coats Land, Antarctica, *Boundary Layer Meteorol.*, *114*, 413–437, doi:10.1007/s10546-004-9564-1.

Zilitinkevich, S. S., V. L. Perov, and J. C. King (2002), Near-surface turbulent fluxes in stable stratification: Calculation techniques for use in general circulation models. *Q. J. Roy. Meteorol. Soc.*, *128*, 1571–1587, doi:10.1002/qj.200212858309.

Zwally, H. J., and S. Fiegles (1994), Extent and duration of Antarctic surface melting, *J. Glaciol.*, *40*, 463–476.

H. Savijärvi and E. Tuovinen, Department of Physics, University of Helsinki, PO Box 64, FI-00014 Helsinki, Finland.

T. Vihma, Meteorological Research, Finnish Meteorological Institute, PO Box 503, FI-00101 Helsinki, Finland. (timo.vihma@fmi.fi)